AGU PUBLICATIONS

Geophysical Research Letters

RESEARCH LETTER
10.1002/2016GL069946

Key Points:
- SMAP and networks of in situ probes observe soil drying after rainfall
- SMAP observes soil drying to occur over a 44% shorter timescale than in situ
- SMAP observes soil drying to occur at twice the rate as in situ

Supporting Information:
- Supporting Information S1
- Table S1

Correspondence to:
P. J. Shellito,
peter.shellito@colorado.edu

Citation:
Shellito, P. J., et al. (2016), SMAP soil moisture drying more rapid than observed in situ following rainfall events, *Geophys. Res. Lett.*, *43*, doi:10.1002/2016GL069946.

Received 7 JUN 2016
Accepted 26 JUL 2016
Accepted article online 29 JUL 2016

SMAP soil moisture drying more rapid than observed in situ following rainfall events

Peter J. Shellito[1], Eric E. Small[1], Andreas Colliander[2], Rajat Bindlish[3], Michael H. Cosh[3], Aaron A. Berg[4], David D. Bosch[5], Todd G. Caldwell[6], David C. Goodrich[7], Heather McNairn[8], John H. Prueger[9], Patrick J. Starks[10], Rogier van der Velde[11], and Jeffrey P. Walker[12]

[1]Department of Geological Sciences, University of Colorado Boulder, Boulder, Colorado, USA, [2]NASA Jet Propulsion Laboratory, California Institute of Technology, Pasadena, California, USA, [3]USDA-ARS Hydrology and Remote Sensing Laboratory, Beltsville, Maryland, USA, [4]Department of Geography, University of Guelph, Guelph, Ontario, Canada, [5]USDA-ARS Southeast Watershed Research Laboratory, Tifton, Georgia, USA, [6]Bureau of Economic Geology, Jackson School of Geosciences, University of Texas at Austin, Austin, Texas, USA, [7]USDA-ARS Southwest Watershed Research Center, Tucson, Arizona, USA, [8]Agriculture and Agri-Food Canada, Ottawa, Ontario, Canada, [9]USDA-ARS National Laboratory for Agriculture and the Environment, Ames, Iowa, USA, [10]USDA-ARS Grazinglands Research Laboratory, El Reno, Oklahoma, USA, [11]Faculty of Geo-Information Science and Earth Observation (ITC), University of Twente, Enschede, Netherlands, [12]Department of Civil Engineering, Monash University, Clayton, Melbourne, Victoria, Australia

Abstract We examine soil drying rates by comparing surface soil moisture observations from the NASA Soil Moisture Active Passive (SMAP) mission to those from networks of in situ probes upscaled to SMAP's sensing footprint. SMAP and upscaled in situ probes record different soil drying dynamics after rainfall. We modeled this process by fitting an exponential curve to 63 drydown events: the median SMAP drying timescale is 44% shorter and the magnitude of drying is 35% greater than in situ measurements. We also calculated drying rates between consecutive observations from 193 events. For 6 days after rainfall, soil moisture from SMAP dries at twice the rate of in situ measurements. Restricting in situ observations to times of SMAP observations does not change the drying timescale, magnitude, or rate. Therefore, observed differences are likely due to differences in sensing depths: SMAP measures shallower soil moisture than in situ probes, especially after rainfall.

1. Introduction

Surface soil moisture exerts an important control on the fluxes of water and energy between the land surface and atmosphere [*Eltahir*, 1998; *Gallego-Elvira et al*., 2016]. It drives land-atmosphere coupling, affecting atmospheric circulation, and regional weather [*Koster et al*., 2004; *Guo et al*., 2006; *Dirmeyer et al*., 2013]. Given these effects, improvements in land surface modeling have been shown to enhance both short-term and seasonal climate forecasting [*Guo et al*., 2011; *Yang et al*., 2011]. Persistence of root zone soil moisture anomalies yields memory in the climate system on scales up to months [*Koster et al*., 2006; *Ghannam et al*., 2016]. Although surface soil moisture varies more rapidly due to the direct effects of precipitation and evaporation [e.g., *Kurc and Small*, 2004], propagation of anomalies from the surface layer influences dynamics throughout the soil profile and below [*Eltahir and Yeh*, 1999]. Observations of soil drying at the surface can therefore inform on deeper, more persistent anomalies that define the onset of drought [*Serafini and Sud*, 1987; *Ford et al*., 2015], affect ecosystem dynamics [*D'Odorico et al*., 2000; *Rodriguez-Iturbe*, 2000; *Daly and Porporato*, 2005], and control soil carbon and nitrogen cycles [*Porporato et al*., 2003; *Ivanov et al*., 2008].

Remote sensing missions such as Soil Moisture Active Passive (SMAP) and Soil Moisture Ocean Salinity (SMOS) have coarse spatial resolution and only pass over a particular location periodically [*Njoku et al*., 2003; *Kerr et al*., 2010; *Entekhabi et al*., 2014]. However, the global coverage of space-borne sensors makes their data optimal for assimilation, allowing for better estimation of root zone soil moisture and hydrometeorologic fluxes [e.g., *Martens et al*., 2016]. To improve this process, efforts must be taken to characterize satellite retrievals.

The science requirement for SMAP (and SMOS) is to provide estimates of soil moisture in the top 5 cm of soil with an unbiased root mean squared error (ubRMSE) no greater than 0.04 $cm^3\,cm^{-3}$ [*Kerr et al*., 2010; *Entekhabi et al*., 2014]. For SMAP validation, in situ soil moisture monitoring sites were developed and charged with providing an estimate of soil moisture over this same depth interval, at a spatial scale commensurate with the SMAP sensing footprint [*Entekhabi et al*., 2014]. For practical reasons, in situ probes in these

networks are typically placed at 5 cm depth, which means they measure soil moisture content between 3.5 and 6.5 cm [*Rondinelli et al*., 2015]. In contrast, L-band radiometers such as that on SMAP measure soil moisture between the surface and a depth that varies. Though nominally 5 cm, penetration depth can be much shallower when soil water content is high [*Njoku and Kong*, 1977; *Escorihuela et al*., 2010; *Jackson et al*., 2012]. In addition, SMAP's soil moisture retrieval algorithm is strictly valid only for uniform soil moisture profiles [*Jackson et al*., 2016], which may not exist immediately following rainfall.

Notwithstanding this imperfect representation of the passive L-band sensing depth, monitoring sites with probes inserted at 5 cm depth have been and continue to be a primary means of validating satellite-based soil moisture estimates [*Jackson et al*., 2010, 2012; *Entekhabi et al*., 2014]. *Chan et al.* [2016] used 13 such sites, referred to as core validation sites (CVS) [*Jackson et al*., 2016], to demonstrate that initial SMAP soil moisture retrievals yield an ubRMSE of 0.038 $cm^3\,cm^{-3}$, thus meeting the mission target. Despite this success, it was qualitatively noted that SMAP soil moisture dries more rapidly than observed in situ [*Chan et al*., 2016], perhaps due to differences in sensing depth between the satellite and in situ observations [*Jackson et al*., 2016].

Two previous studies demonstrated that SMOS soil moisture also decreases more quickly following rainfall than observed in situ. *Champagne et al.* [2016] analyzed data from four sites in Canada (including the two used here) and showed that although SMOS captured drying trends, SMOS soil moisture was often higher than the in situ observations soon after rainfall events. *Rondinelli et al.* [2015], using data from South Fork, Iowa, showed that surface drying rates from SMOS were faster than rates calculated from in situ observations. They used an unsaturated soil water flow model to demonstrate that differences in observation depths could explain the observed differences in drying rates.

This paper contributes to SMAP validation by comparing retrieved soil moisture with in situ observations during soil drying (drydown) events. Data from 193 distinct events across 17 sites with distributed networks of soil moisture probes were used for this analysis. SMAP and in situ soil moisture are both used to calculate (1) exponential timescales of soil drying [e.g., *Kurc and Small*, 2004; *Rondinelli et al*., 2015] and (2) discrete drying rates as a function of time since last rainfall. Calculations are independent of bias and answer a more specific question than ubRMSE can: What differences exist between how SMAP and in situ probes characterize drying of the land surface after a rain event? Analyses include in situ data at both its native high frequency and at the SMAP observation frequency, allowing us to assess if critical information about drying is lost due to the timing and frequency of SMAP observations. Quantifying the accuracy of SMAP drying rates is necessary for informed use of SMAP soil moisture observations.

2. Materials and Methods

2.1. Data

2.1.1. SMAP Observations

The SMAP satellite was launched on 31 January 2015. SMAP overpasses are every 1 to 3 days, with the repeat interval depending on latitude. SMAP's radiometer operates in the L band of the microwave spectrum (1.41 GHz) [*Entekhabi et al*., 2014]. The SMAP radiometer soil moisture team has developed five soil moisture retrieval algorithms to generate level 2 passive soil moisture estimates (L2SMP). This study used the baseline soil moisture algorithm: single channel algorithm using vertical polarization observations (SCAV) [*Chan et al*., 2016]. All SMAP data shown here were processed using a 36 km grid centered on each CVS (described below) and thus differs from the publically available data on the EASE-Grid. We used level 2 descending half-orbit (~6 A.M. local time) observations from 31 March 2015 to 1 March 2016 (data version 3). Data flagged due to frozen conditions, snow, dense vegetation, and precipitation were excluded from the analysis.

2.1.2. In Situ Observations

The SMAP validation program collaborates with CVS situated around the world. These locations constitute an extensive network of densely instrumented soil monitoring sites, allowing rigorous and continual evaluation of SMAP retrievals. Analyses use upscaled data from 17 CVS (Table S1), not individual probe values. Upscaling is based on a geometrically weighted average of probes within the pixel [*Colliander et al*., 2015] that qualifies them for use at the 36 km scale [*Jackson et al*., 2016]. At all sites, probes were inserted horizontally at 5 cm depth, except Yanco and Kyeamba, Australia, where most probes were inserted vertically (0 to 5.8 cm).

In situ data have a sampling frequency of 60 min or less. These data, referred to in our analyses below as $inSitu_{all}$, are assumed to represent the "true" soil moisture drying dynamics at each CVS. Land surface

heterogeneities are averaged out by the upscaling calculation at each site. Network accuracies where quantified are 0.02 $cm^3\ cm^{-3}$ or better [*Cosh et al*., 2004, 2006, 2008; *Bosch et al*., 2006]. Probe random errors average 0.01 $cm^3\ cm^{-3}$ [*Coopersmith et al*., 2016], and probe precision is better than 0.01 $cm^3\ cm^{-3}$ [*Seyfried et al*., 2005]. All analyses were also completed using a subset of in situ observations that correspond in time with SMAP retrievals. This subset of data is referred to as $inSitu_{SMAP}$ (Figure S1 in the supporting information). Temporal resampling isolates the effects of SMAP observation frequency ($inSitu_{all}$ versus $inSitu_{SMAP}$) from overall differences ($inSitu_{all}$ versus SMAP).

2.1.3. Precipitation Products

Precipitation networks are not available at every CVS. In order to ensure a homogenous analysis (gauges, where present, do not have uniformity in number or density), we used Land Data Assimilation System (LDAS) products at all sites. North American LDAS (NLDAS-2) precipitation [*Xia et al*., 2012] covers North American locations, and Global LDAS (GLDAS-1) covers all others [*Rodell and Beaudoing*, 2007]. Analyses employed the one-eighth degree NLDAS-2 or the one-fourth degree GLDAS-1 cell that is most closely aligned with each CVS. The use of such large-scale precipitation products prohibits investigation into possible effects of nonuniform rainfall. In addition, because these products have errors and scale discrepancies, they provided only initial guidance in selecting rain-free intervals. The drydowns were further evaluated and adjusted as follows.

2.2. Selection of Drydown Events

We selected discrete drydown intervals using a two-step process. First, we used LDAS precipitation to automatically identify dry periods that follow rainfall events. The start of such a drydown is designated after 5 mm (or more) of rain has accumulated in the preceding 24 h. The drydown ends once more than 2 mm of subsequent precipitation accumulates. We only consider drydowns that are at least 4 days long. Second, we manually adjusted the drydown start time to within an hour after the observed maximum in situ soil moisture and adjusted the end time to just prior to any increase in soil moisture due to new rainfall. In addition, we excluded events that had obvious errors (sensors dropping in or out), contained fewer than two concurrent SMAP and in situ observations, or demonstrated no response of soil moisture to the rainfall or drydown. The selection process therefore avoided relying exclusively on LDAS products, so using different precipitation data would have minimal impacts on the results.

Using these criteria, 193 drydown events were identified, totaling 2005 days across the 17 CVS (Table S1 and Figures S2–S18). All analyses are limited to observations from these drydown periods, which include 959 SMAP observations and constitute 40% of the snow-free record.

2.3. Analysis Methods

Two methods were used to analyze and compare SMAP observations with in situ observations: (1) fitting of an exponential model to assess the timescale and magnitude of drying and (2) calculation of discrete drying rates between successive observations. Both of these methods provide information in an unbiased framework, so adjusting SMAP time series for bias is unnecessary.

2.3.1. Exponential Model

We modeled the in situ and SMAP observations from individual drydowns as exponential decay functions [*Kurc and Small*, 2004; *Rondinelli et al*., 2015]:

$$\theta(t) = A \times e\left(-\frac{t}{\tau}\right) + \theta_f, \tag{1}$$

where θ is surface soil moisture content ($cm^3\ cm^{-3}$), t is time since the beginning of the drydown (days), and A, τ, and θ_f are empirically determined fitting parameters indicating, respectively, the magnitude of soil moisture drying ($cm^3\ cm^{-3}$), the exponential time constant (days), and a final soil moisture content ($cm^3\ cm^{-3}$; Figure S1). Modeled θ approaches but never reaches θ_f. We therefore constrain θ_f below the lowest soil moisture observed during the drydown and at or above the site's lowest (residual) soil moisture.

For each event, model parameters (τ, A, and θ_f) were selected to minimize the sum of squared errors between modeled soil moisture and (1) $inSitu_{all}$, (2) $inSitu_{SMAP}$, and (3) SMAP observations. Parameter selection used a subspace trust-region algorithm, based on the interior-reflective Newton method [*Coleman and Li*, 1994, 1996].

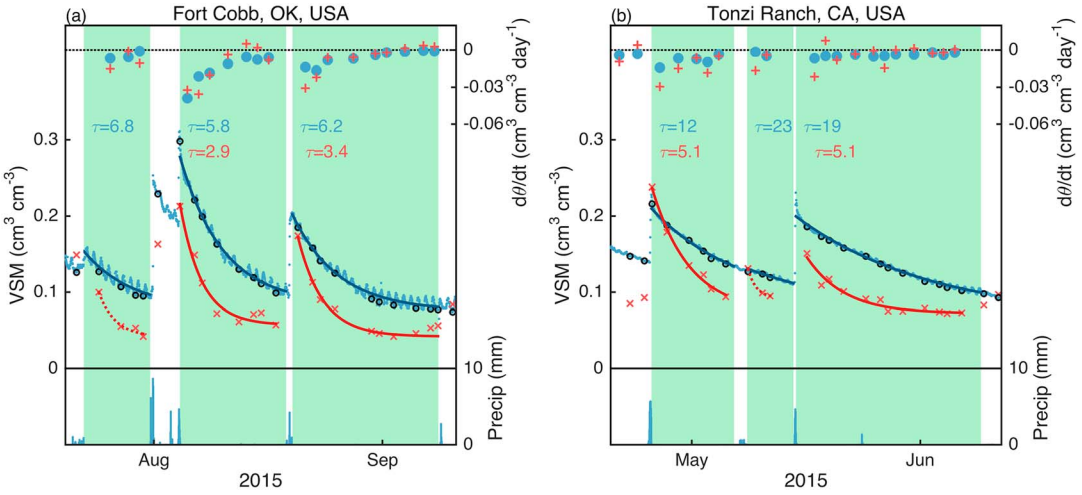

Figure 1. Rainfall (bottom), volumetric soil moisture (VSM; middle), and soil drying rates (top) at (a) Fort Cobb, Oklahoma and (b) Tonzi Ranch, California. Drydowns are highlighted in green. Markers show $\text{inSitu}_{\text{all}}$ (blue dot), $\text{inSitu}_{\text{SMAP}}$ (black circle), and SMAP (red cross) observations. Solid curves are models whose confidence interval around τ does not include zero (acceptable fits). Dotted curves are fitted exponential models whose confidence interval around τ includes zero (low-quality fits). $\text{InSitu}_{\text{SMAP}}$ fits are nearly identical to $\text{inSitu}_{\text{all}}$ fits (Figure S1) and are not shown. τ values for acceptable model fits are displayed according to color.

When fitting equation (1) to the three observation types, confidence intervals at the 68% level were determined, corresponding to one standard deviation. An "acceptable" fit is considered to be one in which the confidence interval around τ does not include zero. Using this criterion, 188 of the 193 models fit to $\text{inSitu}_{\text{all}}$ drydowns were found to be acceptable. Such success indicates that the exponential model provides a reasonable characterization of soil moisture. In contrast, only 88 and 74 models fit to $\text{inSitu}_{\text{SMAP}}$ and SMAP (respectively) were acceptable. This does not indicate that the exponential model is inappropriate for these data but that the lower SMAP observation frequency increases parameter uncertainty. After screening out low-quality fits, there were 63 drydowns that had acceptable model fits to all three observation types. Exponential model results are limited to this subset of drydowns. Widening or narrowing the confidence interval does not significantly alter the results of this study.

2.3.2. Soil Drying Rates

We calculated rates of soil drying ($\mathrm{d}\theta/\mathrm{d}t$) using finite differences within drydown periods:

$$\frac{\mathrm{d}\theta}{\mathrm{d}t} = \frac{\theta_{n+1} - \theta_n}{t_{n+1} - t_n}, \tag{2}$$

where n and $n+1$ correspond to consecutive observations. This analysis required only two or more soil moisture observations within each drydown interval. Thus, unlike the exponential analysis, all 193 drydowns were included. For comparison against SMAP, we use daily in situ data ($\text{inSitu}_{\text{daily}}$), starting 12 h after the drydown commences. This removes the diurnal fluctuations present in $\text{inSitu}_{\text{all}}$. A total of 1807 $\text{inSitu}_{\text{daily}}$ soil drying rates were calculated, across all sites and drydowns. SMAP and $\text{inSitu}_{\text{SMAP}}$ both yielded 769 because of their lower observation frequency.

Drying rates are expected to be most negative at the beginning of a drydown and trend toward zero. To ensure that abnormally infrequent observations did not affect our results, we only calculated drying rates when $t_{n+1} - t_n$ (equation (2)) was three or fewer days. Errors in individual observations introduced considerable noise into the calculated drying rates (Figures 1 and S2–S18). Therefore, each drying rate was binned according to how many days into the drydown interval its midpoint fell, rounded to the nearest whole number day. The results and discussion below are focused on the median value from each bin.

3. Results

For the 2005 drydown days across all sites, the average ubRMSE between SMAP and in situ soil moisture is $0.033\ \mathrm{cm}^3\ \mathrm{cm}^{-3}$, within SMAP mission target accuracy. This is similar to the $0.038\ \mathrm{cm}^3\ \mathrm{cm}^{-3}$ ubRMSE reported by *Chan et al.* [2016] using observations from the full period of record. The four sites with highest ubRMSEs in *Chan et al.* [2016] (carm, sofo, kyea, and reme) all had ubRMSE $> 0.04\ \mathrm{cm}^3\ \mathrm{cm}^{-3}$ in this study as well. By

Table 1. Model Fits, Parameters, and Uncertainties[a]

	Observations Used to Fit Model		
	$\text{InSitu}_{\text{all}}$	$\text{InSitu}_{\text{SMAP}}$	SMAP
RMSE ($cm^3\ cm^{-3}$)	0.0042	0.0020	0.0062
τ (days)	7.33	7.30	4.08
τ uncertainty (days)	0.19	1.30	1.29
A ($100 \times cm^3\ cm^{-3}$)	11.3	11.1	15.2
A uncertainty ($100 \times cm^3\ cm^{-3}$)	0.09	2.1	3.4
θ_f ($100 \times cm^3\ cm^{-3}$)	9.0	9.1	9.2
θ_f uncertainty ($100 \times cm^3\ cm^{-3}$)	0.11	0.84	1.0

[a]Median RMSEs, parameters, and uncertainties for exponential fits to each data type. These data come from 63 drydowns that provide acceptable model fits to all three observation types. A and θ_f values and uncertainties are expressed as $100 \times cm^3\ cm^{-3}$.

comparing timescales and drying rates between SMAP and in situ observations, we can uncover important differences not captured by ubRMSE. All results are summarized using median values to avoid the effects of a positive skew in τ (its range is zero to infinite). Using mean values does not change the findings.

3.1. Exponential Timescales of Soil Drying

The exponential model fits both SMAP and in situ observations of soil moisture following rainfall events (Figure 1): drying is rapid at first and slows with time. The median RMSEs between model fits and observations are well below 0.01 $cm^3\ cm^{-3}$ for all observation types (Table 1). Exponential drying timescales (τ) vary from several to more than 20 days across the 63 events. Investigation into why τ varies from event to event or site to site is beyond the scope of this paper. Possibilities include differences in meteorological conditions, water table depth, vegetation, and soil texture.

τ values fit to SMAP data are consistently smaller than those fit to $\text{inSitu}_{\text{all}}$. For example, the third drydown in Figure 1a has SMAP and $\text{inSitu}_{\text{all}}$ τ values of 3.4 and 6.2 days, respectively. This difference is consistent across nearly all drydowns: of the 63 events with acceptable fits, 53 fall below the 1:1 line in Figure 2a. The median τ value is 44% smaller when fit to SMAP (4.08 days) than when fit to $\text{inSitu}_{\text{all}}$ (7.33 days) (Table 1). Restricting the frequency and timing of in situ observations to that of SMAP does not decrease the exponential drying timescale. Corresponding τ values fit to $\text{inSitu}_{\text{all}}$ and $\text{inSitu}_{\text{SMAP}}$ are centered on the 1:1 line in Figure 2b, and their median values are nearly identical (Table 1).

The magnitude of soil drying, based on A (equation (1)), is 35% greater when estimated from SMAP data than from the complete in situ record ($\text{inSitu}_{\text{all}}$) (Table 1 and Figure S19a). Again, restricting the frequency and timing of in situ observations to that of SMAP does not account for this difference (Figure S19b and Table 1): the A coefficients estimated from $\text{inSitu}_{\text{all}}$ and $\text{inSitu}_{\text{SMAP}}$ are nearly identical.

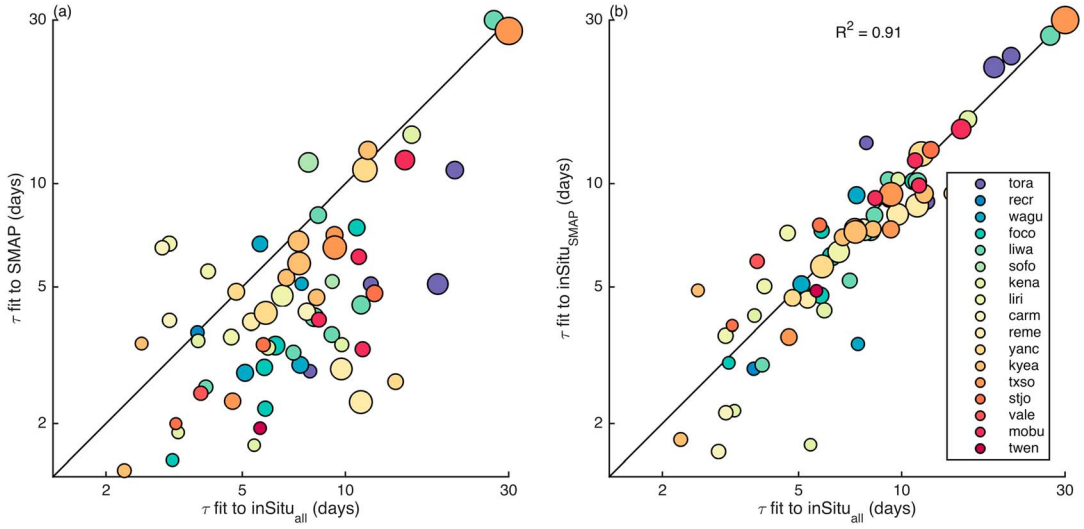

Figure 2. (a) Relationship between $\text{inSitu}_{\text{all}}$-fit and SMAP-fit τ values. (b) Relationship between $\text{inSitu}_{\text{all}}$-fit and $\text{inSitu}_{\text{SMAP}}$-fit τ values. Marker colors correspond to each site as shown. Marker sizes correspond to length of drydown.

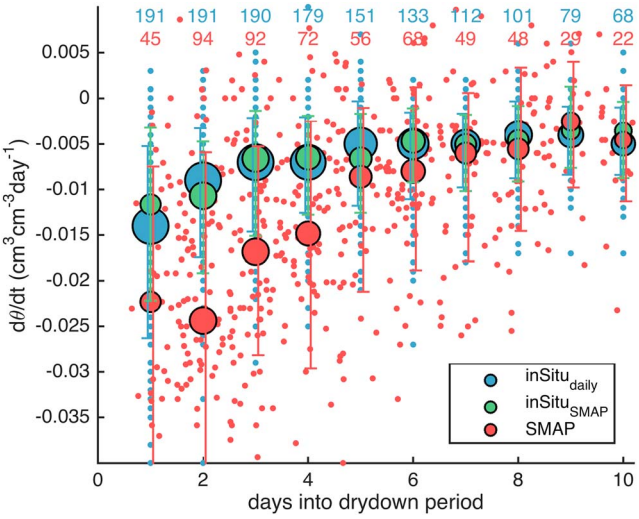

Figure 3. Drying rates calculated from $inSitu_{daily}$ (blue), $inSitu_{SMAP}$ (green), and SMAP (red) as a function of time into the drydown period. Small markers show all data for $inSitu_{daily}$ and SMAP. Large markers show the median of each observation type in each daily bin. Large marker sizes correspond to the number of data points in each bin, which is also shown at the top of the figure. Error bars indicate ±1 standard deviation around the mean (mean not shown).

Parameter uncertainties (Table 1) are primarily related to the number of observations, not how well the exponential model describes the data. Fits to $inSitu_{all}$ have the lowest uncertainty. Models fit to $inSitu_{SMAP}$ and SMAP have the same limited number of observations and similarly high parameter uncertainties due to the challenge of fitting a multiple-parameter model with a limited number of observations.

3.2. Discrete Drying Rates

Figure 3 shows how drying rates vary with increasing time since cessation of rainfall. Data for each site are shown individually in Figures 1 and S2–S18. As expected, the most negative rates (fastest drying) occur soon after rain events. Although there is considerable noise within each daily bin, median values for each day and measurement type reveal two important differences. First, the frequency of soil moisture observations does not affect the calculated drying rate: observations up to 3 days apart ($inSitu_{SMAP}$) yield rates consistent with those calculated from daily data ($inSitu_{daily}$). Second, drying rates are faster when calculated from SMAP than from $inSitu_{daily}$. In days 1 through 6, median drying rates are 1.6, 2.7, 2.4, 2.1, 1.7, and 1.6 times greater, respectively, for SMAP than $inSitu_{daily}$ (mean: 2.0). There is no apparent difference between SMAP and $inSitu_{daily}$ drying rates after day 6. Similar differences exist when SMAP and $inSitu_{SMAP}$ are compared.

The drying rate results are consistent with the exponential model analysis. Compared to $inSitu_{all}$, exponential fits to SMAP exhibit shorter median timescales and greater median magnitudes of drying (Table 1). These differences require that SMAP observes faster drying rates over the interval during which a majority of the soil drying occurs.

4. Discussion and Conclusions

Meeting the SMAP validation goal (ubRMSE $\leq 0.04\ cm^3\ cm^{-3}$) at CVS does not guarantee that the dynamics of drying events determined from SMAP are accurate, especially given the difference in observation depth between satellite radiometer and in situ probes. Quantifying differences that exist is important for both data assimilation applications and model verification studies that utilize SMAP soil moisture.

The exponential model used here characterizes the timescale and magnitude of 63 soil moisture drydowns across 17 sites. The SMAP soil moisture data yield exponential drying timescales that are approximately half (44%) those determined from watershed-averaged in situ observations. In addition, the magnitude of SMAP drying is 35% greater than that of the in situ networks. Direct calculation of drying rates between consecutive observations corroborates that SMAP and in situ soil moisture observations exhibit different behavior. In the 6 days following the rain events (approximately the median exponential drying timescale), surface soil moisture measured by SMAP decreases twice as fast as that measured by in situ probes. Drying rates are effectively equal at longer intervals (>6 days) after rainfall. The differences between SMAP and in situ dynamics are not due to the timing and frequency of SMAP observations; the subset of in situ observations concurrent with SMAP yields nearly identical results as its high-frequency counterpart.

SMAP and in situ probes measure drying behavior differently because they are sensitive to soil moisture at different depths. L-band radiometer measurements are sensitive to soil water between the surface and a moisture-dependent depth, usually 5 cm or less [e.g., *Njoku and Kong*, 1977]. The in situ probes at 15 of the

17 CVS, however, are centered at 5 cm and thus do not measure soil moisture in the top several centimeters [*Rondinelli et al*., 2015]. These differences in sensing depth lead to different characterizations of soil moisture drying. Rain events create positive vertical moisture gradients. The near-surface soil is wetter than deeper soil shortly after rainfall but tends to dry more quickly due to evaporation and vertical redistribution [e.g., *Schneeberger et al*., 2004]. Moreover, L-band sensing depth for very wet soil may be as little as ~1 cm [*Escorihuela et al*., 2010], further accentuating the combined effects of vertical soil moisture gradients and different sensing depths. The two Australia sites yield similar results to those from other sites, despite having vertically inserted probes, possibly because the soil depth observed by the probes is still deeper than SMAP penetration depth. In addition, the sensor head may shelter rain [*Adams et al*., 2015], making probe observations drier than SMAP retrievals until the soil equilibrates.

Results are consistent with those from SMOS [*Rondinelli et al*., 2015; *Champagne et al*., 2016], suggesting that shortened drydowns may be an issue for any L-band instrument. It is also possible that nonuniform rainfall within the validation pixel could lead to different drying dynamics, which should be evaluated in future studies.

Hydrologic applications and studies that utilize SMAP soil moisture must consider the differences in sensing depth, drying timescale, and drying rate discussed here. Our results can help guide efforts to optimize the usefulness of SMAP observations. Bias corrections techniques such as cumulative distribution function matching could potentially minimize differences in drying timescales and rates. Different functions may be needed to relate SMAP and model soil moisture in periods of wetting and drying.

Acknowledgments

This research was supported by NASA grant NNX13AF43G. SMAP data on the validation grid were provided by the SMAP passive soil moisture team members: R. Bindlish, S. Chan, T. Jackson, P. O'Neill, and E. Njoku. Precipitation data used in this study were acquired as part of the mission of NASA's Earth Science Division and archived and distributed by the Goddard Earth Sciences Data and Information Services Center. Thanks to all who have provided high-quality in situ soil moisture data, including Mark Seyfried and the Reynolds Creek Experimental Watershed; Stan Livingston of the St. Joseph's Experimental Watershed (USDA-Agricultural Research Service); José Martínez-Fernández and the REMEDHUS network; Mahta Moghaddam and the Tonzi Ranch SoilSCAPE project; and Ernesto Lopez-Baeza and the Valencia network. The Kenaston network is supported by Environment Canada from grants from the Canadian Space Agency; Tracy Rowlandson and Erica Tetlock are acknowledged for their work with the network. The data used are listed and provided in the supporting information.

References

Adams, J. R., H. McNairn, A. A. Berg, and C. Champagne (2015), Evaluation of near-surface soil moisture data from an AAFC monitoring network in Manitoba, Canada: Implications for L-band satellite validation, *J. Hydrol.*, *521*, 582–592, doi:10.1016/j.jhydrol.2014.10.024.

Bosch, D. D., V. Lakshmi, T. J. Jackson, M. Choi, and J. M. Jacobs (2006), Large scale measurements of soil moisture for validation of remotely sensed data: Georgia soil moisture experiment of 2003, *J. Hydrol.*, *323*(1–4), 120–137, doi:10.1016/j.jhydrol.2005.08.024.

Champagne, C., T. Rowlandson, A. Berg, T. Burns, J. L'Heureux, E. Tetlock, J. R. Adams, H. McNairn, B. Toth, and D. Itenfisu (2016), Satellite surface soil moisture from SMOS and Aquarius: Assessment for applications in agricultural landscapes, *Int. J. Appl. Earth Obs. Geoinf.*, *45*, 143–154, doi:10.1016/j.jag.2015.09.004.

Chan, S. K., et al. (2016), Assessment of the SMAP Passive Soil Moisture Product, *IEEE Trans. Geosci. Remote Sens.*, *54*(8), 4994–5007, doi:10.1109/TGRS.2016.2561938.

Coleman, T. F., and Y. Li (1994), On the convergence of interior-reflective Newton methods for nonlinear minimization subject to bounds, *Math. Program.*, *67*(1), 189–224, doi:10.1007/BF01582221.

Coleman, T. F., and Y. Li (1996), An interior trust region approach for nonlinear minimization subject to bounds, *SIAM J. Optim.*, *6*(2), 418–445, doi:10.1137/0806023.

Colliander, A., et al. (2015), SMAP L2/L3 soil moisture product validation using in situ based core validation sites, Abstract H43H-1626 presented at 2015 Fall Meeting, AGU, San Francisco, Calif., 14–18 Dec.

Coopersmith, E. J., M. H. Cosh, J. E. Bell, and W. T. Crow (2016), Multi-profile analysis of soil moisture within the US Climate Reference Network, *Vadose Zone J.*, *15*(1), doi:10.2136/vzj2015.01.0016.

Cosh, M. H., T. J. Jackson, R. Bindlish, and J. H. Prueger (2004), Watershed scale temporal and spatial stability of soil moisture and its role in validating satellite estimates, *Remote Sens. Environ.*, *92*(4), 427–435, doi:10.1016/j.rse.2004.02.016.

Cosh, M. H., T. J. Jackson, P. Starks, and G. Heathman (2006), Temporal stability of surface soil moisture in the Little Washita River watershed and its applications in satellite soil moisture product validation, *J. Hydrol.*, *323*(1–4), 168–177, doi:10.1016/j.jhydrol.2005.08.020.

Cosh, M. H., T. J. Jackson, S. Moran, and R. Bindlish (2008), Temporal persistence and stability of surface soil moisture in a semi-arid watershed, *Remote Sens. Environ.*, *112*(2), 304–313, doi:10.1016/j.rse.2007.07.001.

Daly, E., and A. Porporato (2005), A review of soil moisture dynamics: From rainfall infiltration to ecosystem response, *Environ. Eng. Sci.*, *22*(1), 9–24, doi:10.1089/ees.2005.22.9.

Dirmeyer, P. A., Y. Jin, B. Singh, and X. Yan (2013), Trends in land–atmosphere interactions from CMIP5 simulations, *J. Hydrometeorol.*, *14*(3), 829–849, doi:10.1175/JHM-D-12-0107.1.

D'Odorico, P., L. Ridolfi, A. Porporato, and I. Rodriguez-Iturbe (2000), Preferential states of seasonal soil moisture: The impact of climate fluctuations, *Water Resour. Res.*, *36*, 2209–2219, doi:10.1029/2000WR900103.

Eltahir, E. A. B. (1998), A soil moisture-rainfall feedback mechanism: 1. Theory and observations, *Water Resour. Res.*, *34*, 765–776, doi:10.1029/97WR03499.

Eltahir, E. A. B., and P. J.-F. Yeh (1999), On the asymmetric response of aquifer water level to floods and droughts in Illinois, *Water Resour. Res.*, *35*, 1199–1217, doi:10.1029/1998WR900071.

Entekhabi, D., et al. (2014), *SMAP handbook—Soil Moisture Active Passive: Mapping Soil Moisture and Freeze/Thaw From Space*, Jet Propulsion Lab., California Inst. Technol., Pasadena, Calif.

Escorihuela, M. J., A. Chanzy, J. P. Wigneron, and Y. H. Kerr (2010), Effective soil moisture sampling depth of L-band radiometry: A case study, *Remote Sens. Environ.*, *114*(5), 995–1001, doi:10.1016/j.rse.2009.12.011.

Ford, T. W., D. B. McRoberts, S. M. Quiring, and R. E. Hall (2015), On the utility of in situ soil moisture observations for flash drought early warning in Oklahoma, USA, *Geophys. Res. Lett.*, *42*, 9790–9798, doi:10.1002/2015GL066600.

Gallego-Elvira, B., C. M. Taylor, P. P. Harris, D. Ghent, K. L. Veal, and S. S. Folwell (2016), Global observational diagnosis of soil moisture control on the land surface energy balance, *Geophys. Res. Lett.*, *43*, 2623–2631, doi:10.1002/2016GL068178.

Ghannam, K., T. Nakai, A. Paschalis, C. A. Oishi, A. Kotani, Y. Igarashi, T. Kumagai, and G. G. Katul (2016), Persistence and memory timescales in root-zone soil moisture dynamics, *Water Resour. Res.*, *52*, 1427–1445, doi:10.1002/2015WR017983.

Guo, Z., et al. (2006), GLACE: The Global Land–Atmosphere Coupling Experiment. Part II: Analysis, *J. Hydrometeorol.*, *7*(4), 611–625, doi:10.1175/JHM511.1.

Guo, Z., P. A. Dirmeyer, and T. DelSole (2011), Land surface impacts on subseasonal and seasonal predictability, *Geophys. Res. Lett.*, *38*, L24812, doi:10.1029/2011GL049945.

Ivanov, V. Y., R. L. Bras, and E. R. Vivoni (2008), Vegetation-hydrology dynamics in complex terrain of semiarid areas: 1. A mechanistic approach to modeling dynamic feedbacks, *Water Resour. Res.*, *44*, W03429, doi:10.1029/2006WR005588.

Jackson, T. J., M. H. Cosh, R. Bindlish, P. J. Starks, D. D. Bosch, M. Seyfried, D. C. Goodrich, M. S. Moran, and J. Du (2010), Validation of advanced microwave scanning radiometer soil moisture products, *IEEE Trans. Geosci. Remote Sens.*, *48*(12), 4256–4272, doi:10.1109/TGRS.2010.2051035.

Jackson, T. J., et al. (2012), Validation of Soil Moisture and Ocean Salinity (SMOS) soil moisture over watershed networks in the U.S., *IEEE Trans. Geosci. Remote Sens.*, *50*(5), 1530–1543, doi:10.1109/TGRS.2011.2168533.

Jackson, T., et al. (2016), Calibration and validation for the L2/3_SM_P version 3 data products, SMAP Project, JPL D-93720, Jet Propulsion Laboratory, Pasadena, CA.

Kerr, Y. H., et al. (2010), The SMOS Mission: New tool for monitoring key elements of the global water cycle, *Proc. IEEE*, *98*(5), 666–687, doi:10.1109/JPROC.2010.2043032.

Koster, R. D., et al. (2004), Regions of strong coupling between soil moisture and precipitation, *Science*, *305*(5687), 1138–1140, doi:10.1126/science.1100217.

Koster, R. D., et al. (2006), GLACE: The Global Land–Atmosphere Coupling Experiment. Part I: Overview, *J. Hydrometeorol.*, *7*(4), 590–610, doi:10.1175/JHM510.1.

Kurc, S. A., and E. E. Small (2004), Dynamics of evapotranspiration in semiarid grassland and shrubland ecosystems during the summer monsoon season, central New Mexico, *Water Resour. Res.*, *40*, W09305, doi:10.1029/2004WR003068.

Martens, B., D. Miralles, H. Lievens, D. Fernández-Prieto, and N. E. C. Verhoest (2016), Improving terrestrial evaporation estimates over continental Australia through assimilation of SMOS soil moisture, *Int. J. Appl. Earth Obs. Geoinf.*, *48*, 146–162, doi:10.1016/j.jag.2015.09.012.

Njoku, E. G., and J.-A. Kong (1977), Theory for passive microwave remote sensing of near-surface soil moisture, *J. Geophys. Res.*, *82*, 3108–3118, doi:10.1029/JB082i020p03108.

Njoku, E. G., T. J. Jackson, V. Lakshmi, T. K. Chan, and S. V. Nghiem (2003), Soil moisture retrieval from AMSR-E, *IEEE Trans. Geosci. Remote Sens.*, *41*(2), 215–229, doi:10.1109/TGRS.2002.808243.

Porporato, A., P. D'Odorico, F. Laio, and I. Rodriguez-Iturbe (2003), Hydrologic controls on soil carbon and nitrogen cycles. I. Modeling scheme, *Adv. Water Resour.*, *26*(1), 45–58, doi:10.1016/S0309-1708(02)00094-5.

Rodell, M., and H. K. Beaudoing (2007), GLDAS Noah Land Surface Model L4 3 hourly 0.25 x 0.25 degree subsetted, version 001, doi:10.5067/F4KOLPJZHKOT.

Rodriguez-Iturbe, I. (2000), Ecohydrology: A hydrologic perspective of climate-soil-vegetation dynamies, *Water Resour. Res.*, *36*, 3–9, doi:10.1029/1999WR900210.

Rondinelli, W. J., B. K. Hornbuckle, J. C. Patton, M. H. Cosh, V. A. Walker, B. D. Carr, and S. D. Logsdon (2015), Different rates of soil drying after rainfall are observed by the SMOS satellite and the South Fork in situ Soil Moisture Network, *J. Hydrometeorol.*, *16*(2), 889–903, doi:10.1175/JHM-D-14-0137.1.

Schneeberger, K., C. Stamm, C. Matzler, and H. Fluhler (2004), Ground-based dual-frequency radiometry of bare soil at high temporal resolution, *IEEE Trans. Geosci. Remote Sens.*, *42*(3), 588–595, doi:10.1109/TGRS.2003.821058.

Serafini, V. V., and Y. C. Sud (1987), The time scale of the soil hydrology using a simple water budget model, *J. Clim.*, *7*(6), 585–591, doi:10.1002/joc.3370070606.

Seyfried, M. S., L. E. Grant, E. Du, and K. Humes (2005), Dielectric loss and calibration of the Hydra Probe soil water sensor, *Vadose Zone J.*, *4*(4), 1070, doi:10.2136/vzj2004.0148.

Xia, Y., et al. (2012), Continental-scale water and energy flux analysis and validation for the North American Land Data Assimilation System project phase 2 (NLDAS-2): 1. Intercomparison and application of model products, *J. Geophys. Res.*, *117*, D03109, doi:10.1029/2011JD016048.

Yang, R., K. Mitchell, J. Meng, and M. Ek (2011), Summer-season forecast experiments with the NCEP climate forecast system using different land models and different initial land states, *J. Clim.*, *24*(9), 2319–2334, doi:10.1175/2010JCLI3797.1.